Evaluating Multi-Objective Algorithms for 3D Basement Topography Inversion from Gravity Data

Arthur A. C. R. Silva, Bruno M. Carvalho, Francisco M. Barboza
Federal University of Rio Grande do Norte - Brazil
arthur.romao@ufrn.br, bruno@dimap.ufrn.br, marcio.barboza@ufrn.br

***Abstract*—The inversion of basement topography from gravimetric data aims to determine the depths of subsurface density contrasts from gravitational anomalies measured by terrestrial or marine instruments. Such inverse problems are inherently ill-posed and highly sensitive to instability. To address these challenges, this study applies and compares three multi-objective optimization algorithms—MOWGN, NSGA-II, and MOPSO—to identify the most effective strategies for extracting geological information from real gravimetric observations. Each algorithm minimizes two competing objectives: the data misfit between observed and calculated anomalies, and a Smoothness (SM) regularization term that stabilizes the inversion process. Implemented in MATLAB, the methods were applied to Bouguer anomaly data from the Recôncavo Basin, northeastern Brazil. The evaluation combined quantitative metrics—hypervolume, C-metric, and computational time—with qualitative analyses of Pareto front distributions, dominance regions, and the geological plausibility of the reconstructed models. Because the data distributions deviated from normality and exhibited heteroscedasticity, nonparametric statistical tests were used: the Mann–Whitney *U* test for pairwise C-metric comparisons, and the Kruskal–Wallis test with Dunn–Bonferroni correction for multiple-group analyses. Overall, the study provides a comprehensive assessment of these algorithms, emphasizing their strengths, limitations, and practical relevance for real-world gravimetric inversion.**

***Keywords*—multi-objective optimization; gravimetry; regularization; computational geophysics.**

I. Introduction

Estimating basement relief from gravimetric data is a fundamental geophysical task that supports the interpretation of subsurface structures and the exploration of natural resources such as hydrocarbons and minerals [1]. However, reconstructing basement topography is challenging due to the ill-posed nature of the inverse problem and the inherent complexity of gravitational signals. To mitigate these issues, modern approaches increasingly employ metaheuristic algorithms and neural networks [2–8].

Inversion problems can be formulated as optimization tasks, where parameters such as interface depths and density contrasts are estimated by minimizing the misfit between observed and modeled data [9]. As noted by Hadamard [10], these problems are ill-posed due to their non-uniqueness and sensitivity to noise amplification. To improve stability and generate geologically plausible solutions, *Smoothness (SM)* regularization is commonly introduced [11].

Multi-Objective Optimization (MOO) addresses problems involving multiple conflicting objectives, generating a Pareto front of non-dominated solutions that represent optimal trade-offs [12, 13]. In basement relief inversion, the competing objectives are typically the minimization of the data misfit and the regularization term, making it a natural multi-objective problem. This study compares three well-established algorithms widely used in geophysical optimization: the *Multi-Objective Weighted Gauss–Newton (MOWGN)*, the *Non-dominated Sorting Genetic Algorithm II (NSGA-II)*, and the *Multi-Objective Particle Swarm Optimization (MOPSO)* [14–18].

MOWGN is a local optimization method that balances the misfit and regularization through Lagrange multipliers, using pseudo-random weights and initial models to explore the Pareto front. Iterative updates are computed using the Jacobian matrix, which quantifies the sensitivity of the objective function to model parameters [19–22].

NSGA-II is a population-based evolutionary algorithm that ranks solutions via Pareto dominance. The use of crossover, mutation, and selection operators promotes diversity, while the NonDominatedSort and CrowdingDistance mechanisms maintain a well-distributed and convergent Pareto front [23].

MOPSO is inspired by swarm intelligence principles, employing dominance-based selection and a grid repository to preserve population diversity. Particles update their positions based on both personal and collective experience, promoting exploration and convergence along the Pareto front [24].

Algorithmic performance was evaluated using two main criteria: (i) *solution quality*, measured by the hypervolume and C-metric indicators, and (ii) *computational efficiency*, measured by the total execution time. Together, these metrics provide a robust framework for assessing each algorithm's capability to reconstruct complex geological structures from real gravimetric data [25–29].

This study presents a comprehensive methodology for three-dimensional basement relief delineation that integrates global and local optimization strategies. By incorporating stabilizing constraints within a multi-objective inversion framework, the proposed approach enhances solution reliability, improves geological consistency, and provides meaningful insights for practical applications in gravimetric interpretation and basin modeling.

II. *MOO* Framework

MOO involves the simultaneous optimization of two or more, often conflicting, objective functions. In geophysical inversion, the joint minimization of the data misfit and a stabilizing regularization term naturally leads to a multi-objective formulation.

Formally, a general *MOO* problem can be expressed as:

$$\mathbf{F}(\mathbf{d}) = [F_1(\mathbf{d}), F_2(\mathbf{d}), \ldots, F_K(\mathbf{d})],$$

where $\mathbf{d} = (d_1, d_2, \ldots, d_N) \in D \subset \mathbb{R}^N$ denotes the vector of decision variables, and each $F_i(\mathbf{d})$ is a scalar objective function. The feasible domain D is defined by bounds and constraints:

$$\begin{aligned} \min_{\mathbf{d}\in D} \quad & \mathbf{F}(\mathbf{d}) = [F_1(\mathbf{d}), \ldots, F_K(\mathbf{d})] \\ \text{subject to:} \quad & g_t(\mathbf{d}) \leq 0, \quad t = 1, \ldots, P; \\ & h_r(\mathbf{d}) = 0, \quad r = 1, \ldots, Q; \\ & d_i^L \leq d_i \leq d_i^U, \quad i = 1, \ldots, N, \end{aligned} \tag{1}$$

where $g_t(\mathbf{d})$ and $h_r(\mathbf{d})$ represent inequality and equality constraint functions, respectively; P and Q denote the number of inequality and equality constraints; and d_i^L and d_i^U are the lower and upper bounds of the i-th decision variable.

For basement relief inversion, the problem is typically bi-objective: minimizing the gravity data misfit $\Im(\mathbf{d})$ and a regularization term $\aleph(\mathbf{d})$ that ensures smoothness and stability:

$$\begin{aligned} & \min_{\mathbf{d}\in D} \ \mathbf{F}(\mathbf{d}) = [\Im(\mathbf{d}), \aleph(\mathbf{d})] \\ & \text{subject to:} \quad \mathbf{d}_i^L \leq \mathbf{d}_i \leq \mathbf{d}_i^U, \quad i = 1, \ldots, N \end{aligned} \tag{2}$$

This approach allows exploring the entire Pareto front, showing trade-offs between competing objectives without relying on arbitrary weighting. It also improves interpretability, as solutions along the Pareto front may represent geologically plausible alternatives. Instead of a single "best" model, MOO provides a set of viable solutions that support more robust and transparent geological interpretations.

A. Forward Model

The forward model predicts the gravity field generated by a hypothesized subsurface structure. In basement topography studies, it computes the theoretical gravity anomaly vector $\mathbf{g}^{\text{obs}}$ from a depth vector $\mathbf{d}$ describing the basin geometry.

1) Three-Dimensional Forward Modeling: In three dimensions, the basin and basement are divided into voxels—rectangular prisms of fixed density ρ—defined by corner coordinates (x_m, y_m, z_m) and (x_M, y_M, z_M). For an observation point $P(x_p, y_p, z_p)$, the relative coordinates are:

$$\begin{aligned} (x_1, y_1, z_1) &= (x_m, y_m, z_m) - (x_p, y_p, z_p), \\ (x_2, y_2, z_2) &= (x_M, y_M, z_M) - (x_p, y_p, z_p). \end{aligned}$$

The gravitational effect of each voxel is approximated analytically [30, 31] as:

$$g(d_i) = \sum_{i=1}^{N} \sum_{j=1}^{M} f_{ij}(\rho, r_{ij}), \tag{3}$$

$$\begin{aligned} f(\rho, r) = & G\rho\, \Delta x\, \Delta y\, \Delta z \cdot \\ & \left[\frac{1}{r^2} + \frac{5}{24r^6}(V_1 + V_2 + V_3) \left(1 - \frac{2r^2}{5z^2}\right) \right] \frac{z}{r}, \end{aligned} \tag{4}$$

where:

$$\begin{aligned} & V_1 = (2\Delta x^2 - \Delta y^2 - \Delta z^2)x^2, \quad V_2 = (2\Delta y^2 - \Delta x^2 - \Delta z^2)y^2, \\ & V_3 = (2\Delta z^2 - \Delta x^2 - \Delta y^2)z^2, \qquad r = \sqrt{x^2 + y^2 + z^2}. \end{aligned}$$

Summing all voxel contributions yields the total gravity response at the surface. This modeling step is essential for the inversion process that reconstructs the subsurface basement geometry.

B. Data Misfit Functional

The data misfit functional quantifies the discrepancy between observed and modeled gravity data:

$$\Im(\mathbf{d}) = \frac{1}{m} \left\| \mathbf{g}^{\text{obs}} - \mathbf{g}(\mathbf{d}) \right\|_2^2, \tag{5}$$

where $\mathbf{g}^{\text{obs}}$ is the observed gravity vector and $\mathbf{g}(\mathbf{d})$ is the predicted response from the forward model. The normalization by $1/m$ scales the misfit by the number of data points, allowing comparison across datasets.

C. Regularization for Stabilization

Because gravity inversion is ill-posed, minimizing only the misfit leads to unstable and non-unique solutions. Regularization introduces additional constraints that enforce smoothness and physical plausibility [32, 33].

1) SM Regularization: SM regularization penalizes abrupt spatial variations, promoting gradual depth changes. Using the finite-difference operator $\mathcal{D}$, the discrete form is denoted by:

$$\aleph_{\text{smooth}}(\mathbf{d}) = \left\| \mathcal{D}\,\mathbf{d} \right\|_2^2. \tag{6}$$

This helps suppress unrealistic oscillations and produces geologically consistent basement relief models [34, 35].

D. Optimization Methods

Three *MOO* algorithms were applied to minimize the data misfit and regularization terms simultaneously:

1) *MOWGN*;
2) *NSGA-II*;
3) *MOPSO*.

Each algorithm follows a distinct strategy to approximate the Pareto front and identify trade-off solutions between the objectives. Their main steps are summarized in the pseudocodes of Algorithms 1, 2, and 3.

Algorithm 1: *MOWGN* for Multi-Objective Inversion

Input: Initial model $\mathbf{d}_0$, observed data $\mathbf{g}^{obs}$, smoothness matrix $\mathcal{D}$, forward model $\mathbf{g}(\mathbf{d})$, perturbation γ, number of solutions η;
Output: Pareto set $\{\mathbf{d}_1, \dots, \mathbf{d}_\eta\}$;
Generate η interpolated weights $\mathbf{w}$;
for $i = 1$ ***to*** η **do**
  Set $\mathbf{d} \leftarrow \mathbf{d}_0$;
  while *not converged* **do**
    Compute Jacobian $\mathbf{G}$ using finite differences;
    Update model:
    $\Delta\mathbf{d} = (\mathbf{G}^T\mathbf{G} + w_i\mathcal{D}^T\mathcal{D})^{-1}\mathbf{G}^T(\mathbf{g}^{obs} - \mathbf{g}(\mathbf{d}))$;
    $\mathbf{d} \leftarrow \mathbf{d} + \Delta\mathbf{d}$;
  end
  Store $\mathbf{d}_i = \mathbf{d}$;
end
return $\{\mathbf{d}_1, \dots, \mathbf{d}_\eta\}$

1) MOWGN: MOWGN extends the classical Gauss-Newton method to handle multiple objectives. It iteratively minimizes a weighted combination of the objectives using the Jacobian matrix and second-order approximations. The process is repeated for different weights (w_i) to generate a set of Pareto-optimal models (Algorithm 1).

2) NSGA-II: NSGA-II is an evolutionary algorithm that combines non-dominated sorting, elitism, and crowding distance to maintain solution diversity. It evolves a population through crossover and mutation, selecting the best non-dominated individuals in each generation (Algorithm 2).

Algorithm 2: *NSGA-II* for Multi-Objective Inversion

Input: Population size η, generations Γ, crossover p_c, mutation p_m, bounds $[lb, ub]$, objective function $\mathbf{F}(\mathbf{d})$;
Output: Pareto set $\{\mathbf{d}_1, \dots, \mathbf{d}_\eta\}$;
Generate initial population $\mathcal{P}_0$ within $[lb, ub]$;
Evaluate $\mathbf{F}(\mathbf{d})$ for all individuals;
for $\tau = 1$ ***to*** Γ **do**
  Perform non-dominated sorting and compute crowding distances;
  Generate offspring via crossover and mutation;
  Evaluate offspring objectives;
  Combine and select top η individuals;
end
return *Non-dominated set from final population*

3) MOPSO: MOPSO extends *Particle Swarm Optimization (PSO)* to multiple objectives using a repository of non-dominated solutions and a grid-based strategy to maintain diversity. Each particle updates its position based on inertia, personal best, and leaders selected from the repository (Algorithm 3).

Algorithm 3: *MOPSO* for Multi-Objective Inversion

Input: Population size η, iterations Γ, inertia ω, coefficients ϕ_1, ϕ_2, mutation probability μ, bounds $[lb, ub]$, repository size ρ, grid divisions ν;
Output: Repository of Pareto solutions $\mathcal{R}$;
Initialize particles and evaluate $\mathbf{F}(\mathbf{d})$;
Initialize repository $\mathcal{R}$ with non-dominated solutions;
for $\tau = 1$ ***to*** Γ **do**
  foreach *particle* $\mathbf{d}_i$ **do**
    Select leader from $\mathcal{R}$;
    Update velocity and position;
    Evaluate $\mathbf{F}(\mathbf{d}_i)$ and update personal best;
  end
  Apply mutation with probability μ;
  Update repository $\mathcal{R}$ and prune if $|\mathcal{R}| > \rho$;
end
return *Final repository* $\mathcal{R}$

III. METHODOLOGY

The computational experiments were carried out using a real three-dimensional (3D) geological model representing the Recôncavo Basin, located in northeastern Brazil. In this case study, key control parameters were systematically adjusted and optimized using three *MOO* algorithms: the *MOWGN*, the *NSGA-II*, and the *MOPSO*.

Each experiment started from an initial geological model defined by estimated basement depths, which was iteratively refined throughout the optimization process. This procedure allowed the assessment of each algorithm's capability to balance conflicting objectives—specifically, minimizing the data misfit while ensuring smoothness in the estimated basement relief. The adopted framework also enabled a comprehensive evaluation of the robustness and generalization performance of the algorithms when applied to real gravimetric data.

Recôncavo Basin

The Recôncavo Basin is a classic example of a graben-type depression forming part of the Recôncavo–Tucano–Jatobá aborted rift system. This rift developed during the Upper Cretaceous as a direct consequence of the South Atlantic opening, representing a fundamental component of the Brazilian intracontinental rift network associated with the breakup of Gondwana [36]. Due to its well-established tectonic and stratigraphic evolution, the Recôncavo Basin is considered one of the most representative extensional basins in South America.

The Bouguer anomaly distribution across the basin exhibits pronounced lateral variations associated with fault-bounded structural blocks and irregularities in basement topography [37]. These variations reflect the basin's tectonic framework and provide valuable constraints for the inversion procedure.

Figure 1 shows the Bouguer anomaly model of the Recôncavo Basin used as a reference for comparison.

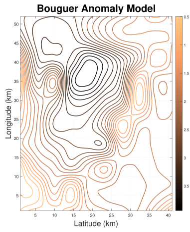

Figure 1. Contour representation of the Bouguer anomaly model of the Recôncavo Basin.

The discretized basin model consisted of $n = 100$ rectangular prisms arranged in a 10×10 grid. Each prism had a vertical thickness of 3 km, covering a total lateral extent of approximately 52 km (north–south) by 41 km (east–west). A constant density contrast of $\rho = -0.2750$ g/cm^3 was assumed, and $m = 889$ gravity anomaly observations were used during the inversion process.

The algorithmic configurations for the Recôncavo Basin were carefully defined to account for the region's large spatial extent and geological heterogeneity. Each method was experimentally fine-tuned to ensure stable convergence and effective exploration of the search space. The initial model d_0 was derived from the Bouguer anomaly and used to define the search bounds for both *NSGA-II* and *MOPSO*, with $k_{\min} = 0.5$ and $k_{\max} = 1.5$. In addition, both algorithms employed a population size $\eta = 500$ and a maximum number of iterations $\Gamma = 500$. *MOWGN* was configured with a maximum of 10 iterations, a Pareto front size $\Omega = 175$, and a weight vector $\mathbf{w}$ composed of random values drawn from the range $[100, 1000]$. *NSGA-II* used a mutation rate $p_m = 0.01$, crossover rate $p_c = 0.75$, mutation factor $\kappa = 0.1$, and tournament size $\xi = 3$. Finally, *MOPSO* employed a repository size $\rho = 175$, grid divisions $\nu = 20$, acceleration coefficients $\phi_1 = 2$ and $\phi_2 = 2$, inertia weight $\omega = 1$, mutation rate $\mu = 0.1$, and maximum velocity $v_{\max} = 0.2 \cdot (ub - lb)$.

The integration of real gravimetric data provided a consistent and comprehensive framework for evaluating the performance of the proposed multi-objective inversion methodology. The Recôncavo Basin case study represented a particularly challenging benchmark due to its complex geological framework, highly irregular basement morphology, and the pronounced spatial variability of the observed gravity field.

IV. Results and Discussion

The performance of the algorithms was evaluated through both quantitative and qualitative analyses applied exclusively to the real gravimetric dataset from the Recôncavo Basin, located in northeastern Brazil. The inversion aimed to reconstruct the three-dimensional basement relief of the basin from observed Bouguer anomalies, ensuring geological consistency while minimizing the data misfit and preserving smoothness in the estimated subsurface structures.

A. *Quantitative Analysis*

In the quantitative analysis, three complementary criteria were adopted: (i) the **hypervolume** indicator, which measures the convergence and diversity of Pareto-optimal solutions; (ii) the **C-metric**, which quantifies the dominance relationship among Pareto fronts; and (iii) the **computational efficiency**, expressed by the total execution time required to obtain the approximate Pareto sets.

Statistical validation was performed using non-parametric hypothesis tests with a significance level of $\alpha = 0.05$. Since the assumptions of normality and homogeneity of variance were not satisfied, the Kruskal–Wallis and Mann–Whitney U tests were applied, followed by the Dunn–Bonferroni post-hoc correction when necessary.

Hypervolume: The hypervolume results revealed statistically significant differences among the algorithms ($p = 0.0160$). The Dunn–Bonferroni post-hoc test indicated that these differences were primarily between *MOWGN* and *NSGA-II* ($p = 0.0144$). Figure 2 presents the Pareto fronts obtained by each algorithm with respect to the reference point used for hypervolume computation. These Pareto fronts were constructed from ten independent runs of each algorithm; all ten fronts were combined, and dominated solutions were subsequently removed to form the final composite Pareto fronts.

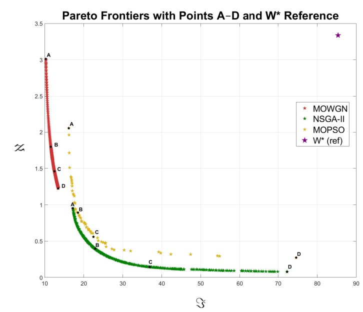

Figure 2. Pareto fronts with representative points of the *MOWGN*, *NSGA-II*, and *MOPSO* algorithms for the Recôncavo Basin.

Based on the median hypervolume values, the ranking was as follows: *NSGA-II* (88.7319), *MOPSO* (38.6440), and *MOWGN* (20.2386). These results demonstrate the superior ability of *NSGA-II* to manage trade-offs between objectives, achieving a more diverse and convergent set of solutions in the real data inversion scenario.

C-Metric: The C-metric evaluated the dominance relationships between Pareto fronts. The Mann–Whitney test revealed that *NSGA-II* and *MOWGN* did not significantly dominate each other ($p = 1.0000$), while both significantly dominated *MOPSO* ($p = 0.0001$). This outcome confirms that *NSGA-II* and *MOWGN* achieved better front coverage and higher solution quality compared to *MOPSO*, which tended to produce solutions concentrated in limited regions of the objective space.

Computational Efficiency: Regarding computational time, significant differences were observed among the algorithms ($p = 0.0000$). According to the Dunn–Bonferroni test, *MOWGN* was significantly faster than both *NSGA-II* and *MOPSO*. The median computational times were 3,132.21, 4,007.34 and 4,218.72 seconds, for the **MOWGN**, **NSGA-II** and **MOPSO**, respectively.

The deterministic nature of *MOWGN*, combined with its gradient-based structure, resulted in faster convergence, whereas the population-based heuristics (*NSGA-II* and *MOPSO*) required more iterations to achieve satisfactory Pareto approximations.

B. Qualitative Analysis

The qualitative analysis focused on the geological plausibility and spatial consistency of the reconstructed basement reliefs. The non-dominated solutions from each algorithm were merged, and representative points along the Pareto fronts were selected for visualization and interpretation. The contour maps illustrate how effectively each method reproduced the basin's structural configuration and depth variations.

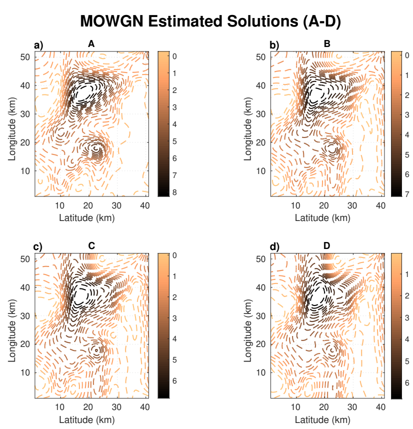

Figure 3. Contour visualization of *MOWGN* estimated solutions.

MOWGN: The *MOWGN* algorithm achieved satisfactory convergence and produced a well-distributed Pareto front, evidencing its capacity to explore diverse trade-offs between the data misfit and smoothness objectives. The contour visualization (Figure 3), with representative points corresponding to those in Figure 2, shows that the reconstructed basement relief effectively captured the main tectonic and morphological features of the basin. The estimated surface exhibited coherent structural trends and avoided spurious oscillations, reflecting the stabilizing influence of the regularization term.

NSGA-II: The *NSGA-II* algorithm exhibited excellent convergence and diversity, with balanced trade-offs across the Pareto front. Its estimated basement reliefs (Figure 4), with representative points corresponding to those in Figure 2, preserved the principal stratigraphic and structural patterns of the Recôncavo Basin, showing smooth depth transitions and well-defined fault-related depressions. The results highlight the algorithm's strong capacity for global exploration while maintaining fine local adjustments.

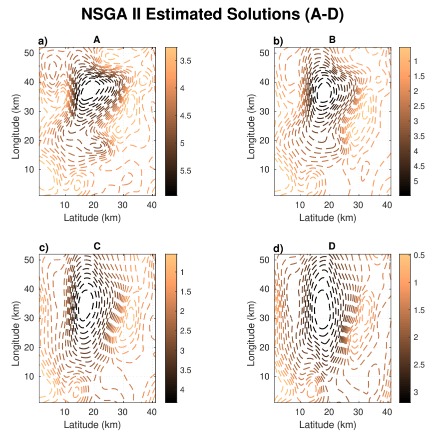

Figure 4. Contour visualization of *NSGA-II* estimated solutions.

MOPSO: The *MOPSO* algorithm reached acceptable convergence, with its best solutions concentrated near the knee region of the Pareto front. Although some smoothing effects were observed, the reconstructed reliefs (Figure 5), with representative points corresponding to those in Figure 2, reproduced the main morphological trends of the basin, including the central depression and the flanking structural highs.

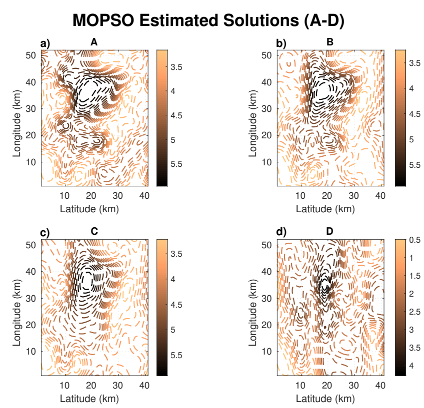

Figure 5. Contour visualization of *MOPSO* estimated solutions.

Despite its slightly higher computational cost and lower diversity compared to *NSGA-II*, *MOPSO* demonstrated robustness and consistency, successfully reproducing the main tectonic features and maintaining geological plausibility in the reconstructed basement model. These results confirm the algorithm's potential for real-world gravimetric inversion problems where trade-off management between precision and smoothness is essential.

V. Conclusion

This study assessed the performance of three *MOO* algorithms—*MOWGN*, *NSGA-II*, and *MOPSO*—for the inversion of gravimetric data from the Recôncavo Basin. The inverse problem was formulated as a bi-objective task designed to simultaneously minimize the data misfit and the first-order Tikhonov regularization term, ensuring both accuracy and smoothness in the reconstructed basement relief.

- **Hypervolume:** *NSGA-II* achieved the highest performance (88.73), followed by *MOPSO* (38.64) and *MOWGN* (20.23).
- **C-Metric:** *NSGA-II* and *MOWGN* showed comparable dominance relationships, both outperforming *MOPSO*.
- **Computational Efficiency:** *MOWGN* was the fastest (3132 s), followed by *NSGA-II* (4007 s) and *MOPSO* (4218 s).

All algorithms produced geologically consistent models of the basin's basement relief. *NSGA-II* demonstrated the best overall accuracy and stability, effectively delineating the major structural and stratigraphic features of the Recôncavo Basin. *MOWGN* stood out for its computational efficiency and well-distributed Pareto fronts, making it a suitable choice for preliminary or time-sensitive analyses. *MOPSO*, despite exhibiting moderate smoothing, achieved stable convergence and satisfactory morphological reconstruction.

In summary, *NSGA-II* proved to be the most robust and balanced algorithm, combining high-quality solutions with strong geological plausibility. *MOWGN* offered a faster yet reliable alternative, while *MOPSO* provided consistent results with lower computational precision.

Future research should focus on developing hybrid or adaptive strategies that integrate the rapid convergence of *MOWGN* with the global search capability of *NSGA-II*. Such approaches may further enhance Pareto diversity, reconstruction accuracy, and computational efficiency in large-scale geophysical inversion problems.

Acknowledgements

This study was financed in part by the Coordenação de Aperfeiçoamento de Pessoal de Nível Superior - Brasil (CAPES) - Finance Code 001.

References

[1] W. M. Telford, L. P. Geldart, and R. E. Sheriff, *Applied Geophysics*. Cambridge University Press, 1990.

[2] M. A. Al-Garni, "Inversion of residual gravity anomalies using neural network," *Arabian J. Geosci.*, vol. 6, pp. 1509–1516, 2013.

[3] J. Pallero *et al.*, "Gravity inversion and uncertainty assessment of basement relief via particle swarm optimization," *J. Appl. Geophys.*, vol. 116, pp. 180–191, 2015.

[4] ——, "3D gravity inversion and uncertainty assessment of basement relief via particle swarm optimization," *J. Appl. Geophys.*, vol. 139, pp. 338–350, 2017.

[5] A. Joolaei *et al.*, "Basement relief modeling by gravity inversion via ant colony algorithm," *Iran. J. of Geophys.*, vol. 14, no. 1, pp. 39–54, 2020.

[6] S. He *et al.*, "Recovering 3D basement relief using gravity data through convolutional neural networks," *J. Geophys. Res.: Solid Earth*, vol. 126, no. 10, p. e2021JB022611, 2021.

[7] Q. Yang *et al.*, "3-D gravity inversion based on deep convolution neural networks," *IEEE Geosci. Remote Sens. Lett.*, vol. 19, pp. 1–5, 2021.

[8] C. Dubey *et al.*, "Basement relief of sedimentary basin using gravity data from deep neural network approach," *J Geol Geophys*, vol. 12, p. 1066, 2023.

[9] M. K. Sen and P. L. Stoffa, *Global Optimization Methods in Geophysical Inversion*. Cambridge Univ. Press, 2013.

[10] J. Hadamard, "Sur les problèmes aux dérivées partielles et leur signification physique," 1902, princeton Univ. Bull., pages 49–52.

[11] A. N. Tikhonov, "On the solution of incorrectly stated problems and a method of regularization," in *Dokl. Acad. Nauk. SSSR*, vol. 151, 1963, pp. 501–504.

[12] J. L. Cohon, *Multiobjective Programming and Planning*. Courier Corporation, 2013.

[13] K. Deb, *Multiobjective Optimization Using Evolutionary Algorithms*. New York: Wiley, 2001.

[14] J. Xiong and T. Zhang, "Multiobjective particle swarm inversion algorithm for two-dimensional magnetic data," *Appl. Geophys.*, vol. 12, no. 2, pp. 127–136, 2015.

[15] S. Schnaidt *et al.*, "Pareto-optimal multi-objective inversion of geophysical data," *Pure Appl. Geophys.*, vol. 175, no. 6, pp. 2221–2236, 2018.

[16] F. Pace *et al.*, "Joint optimization of geophysical data using multi-objective swarm intelligence," *Geophys. J. Int.*, vol. 218, no. 3, pp. 1502–1521, 2019.

[17] F. M. Barboza, A. A. d. C. R. E. Silva, and B. M. Carvalho, "2D basement relief inversion using sparse regularization," https://arxiv.org/abs/2410.14942, 2024, arXiv.

[18] R. Sharma *et al.*, "Joint inversion of DC resistivity and MT data using multi-objective grey wolf optimization," in *NSG 2024 30th Eur. Meet. of Environm. and Engin. Geophys.*, vol. 2024, 2024, pp. 1–5.

[19] M. A. Meju, *Geophysical Data Analysis: Understanding Inverse Problem Theory and Practice*. Soc. Explor. Geophys., 1994.

[20] W. Murray, M. H. Wright, and P. E. Gill, *Practical Optimization*. SIAM-Soc. Ind. and Appl. Math., 2019.

[21] P. C. Hansen, "The L-curve and its use in the numerical treatment of inverse problems," IMM, Tech. Univ. of Denmark, Tech. Rep. IMM-REP-1999-15, 1999.

[22] D. P. Bertsekas, *Constrained Optimization and Lagrange Multiplier Methods*. Acad. Press, 2014.

[23] K. Deb *et al.*, "A fast and elitist multiobjective genetic algorithm: NSGA-II," *IEEE Trans. Evol. Comput.*, vol. 6, no. 2, pp. 182–197, 2002.

[24] C. C. Coello and M. S. Lechuga, "MOPSO: A proposal for multiple objective particle swarm optimization," in *Proc. of CEC'02*, vol. 2. IEEE, 2002, pp. 1051–1056.

[25] E. Zitzler, "Evolutionary algorithms for multiobjective optimization," in *Evolutionary Methods for Design, Optimization and Control*, K. Giannakoglou *et al.*, Eds. Barcelona, Spain: CIMNE, 1998.

[26] ——, *Evolutionary Algorithms for Multiobjective Optimization: Methods and Applications*. Shaker Ithaca, 1999, vol. 63.

[27] W. H. Kruskal and W. A. Wallis, "Use of ranks in one-criterion variance analysis," *J. Am. Stat. Assoc.*, vol. 47, no. 260, pp. 583–621, 1952.

[28] O. J. Dunn, "Multiple comparisons using rank sums," *Technom.*, vol. 6, no. 3, pp. 241–252, 1964.

[29] M. Hollander, D. A. Wolfe, and E. Chicken, *Nonparametric Statistical Methods*. John Wiley & Sons, 2013.

[30] J. Fullea, M. Fernandez, and H. Zeyen, "FA2BOUG—A FORTRAN 90 code to compute bouguer gravity anomalies from gridded free-air anomalies: Application to the Atlantic-Mediterranean transition zone," *Comput. Geosci.*, vol. 34, no. 12, pp. 1665–1681, 2008.

[31] W. D. MacMillan, *The Theory of the Potential*. New York: Dover Publications, 1958, 2nd edition.

[32] A. N. Tikhonov and V. Y. Arsenin, *Solutions of Ill-posed Problems*. New York: John Wiley & Sons, 1977, vol. 1.

[33] H. W. Engl, M. Hanke, and A. Neubauer, *Regularization of Inverse Problems*. Springer Sci. & Bus. Media, 1996, vol. 375.

[34] W. A. Lima, "Inversão gravimétrica do relevo de bacias extencionais através da variação total," Master's thesis, PPgG, Instituto de Geociências, 2009.

[35] F. M. Barboza, W. E. Medeiros, and J. M. Santana, "A user-driven feedback approach for 2D direct current resistivity inversion based on particle swarm optimization," *Geophys.*, vol. 84, no. 2, pp. E105–E124, 2019.

[36] V. C. F. Barbosa, "Mapeamento do relevo do embasamento de bacias sedimentares através da inversão gravimétrica vinculada," Ph.D. dissertation, UFPA, 1998.

[37] J. W. Leão *et al.*, "Gravity inversion of basement relief constrained by the knowledge of depth at isolated points," *Geophys.*, vol. 61, no. 6, pp. 1702–1714, 1996.